Trim38 attenuates pressure overload-induced cardiac hypertrophy by suppressing the TAK1/JNK/P38 signaling pathway

YANAN PANG[1,2*], LUYAO WU[3*], JIACHUN XIA[3*], XIN XU[4], CHENSHAN GAO[3], LEI HOU[2] and LI JIANG[1]

[1]Institute of Cardiovascular Diseases, Tongren Hospital, Shanghai Jiao Tong University School of Medicine, Shanghai 200336, P.R. China; [2]Department of Cardiology, Songjiang Hospital Affiliated to Shanghai Jiaotong University School of Medicine, Shanghai 201600, P.R. China; [3]Division of Cardiology, Tongren Hospital, Shanghai Jiao Tong University School of Medicine, Shanghai 200336, P.R. China; [4]Collaborative Innovation Centre of Regenerative Medicine and Medical Bioresource Development and Application Co-constructed by The Province and Ministry, Guangxi Medical University, Nanning, Guangxi 530021, P.R. China

Received April 26, 2024; Accepted February 20, 2025

DOI: 10.3892/ijmm.2025.5539

Abstract. Pathological cardiac hypertrophy is a major contributor to heart failure (HF), resulting in high mortality rates worldwide; therefore, identifying key molecules in pathological cardiac hypertrophy is of critical importance for preventing or reversing HF. Tripartite motif 38 (Trim38) is an E3 ubiquitin ligase that serves a pivotal role in various diseases. The present study aimed to elucidate the regulatory role of Trim38 in pressure overload-induced pathological cardiac hypertrophy and to explore its underlying molecular mechanisms. The expression of Trim38 was decreased in hypertrophic heart tissues from a murine model of transverse aortic constriction (TAC) and in neonatal rat cardiomyocytes (NRCMs) treated with phenylephrine (PE). Furthermore, Trim38 knockout (Trim38-KO) aggravated cardiac hypertrophy after TAC, and Trim38 knockdown in cardiomyocytes increased cell cross section area, and upregulated the expression of atrial natriuretic peptide (ANP) and brain natriuretic peptide (BNP) following treatment with PE. Ubiquitinomics analysis revealed that the MAPK signaling pathway was regulated by Trim38. Furthermore, western blotting confirmed that Trim38-KO activated TAK1 and JNK/P38. By contrast, Trim38 overexpression in NRCMs suppressed the JNK/P38 signaling pathway and inhibited the phosphorylation of TAK1. Furthermore, Trim38 knockdown resulted in a marked enhancement of TAK1 phosphorylation, concomitant with an augmentation of cardiomyocyte area and a significant upregulation of the hypertrophic biomarkers ANP and BNP. By contrast, infection with an adenovirus containing dominant-negative TAK1 inhibited TAK1 activity, which attenuated Trim38 knockdown-induced cardiomyocyte hypertrophy, confirming that TAK1 is a key molecule involved in the protective effects of Trim38 on cardiomyocytes. In conclusion, to the best of our knowledge, the present study is the first to reveal that Trim38 confers protection against pathological cardiac hypertrophy by inhibiting the TAK1/JNK/P38 signaling pathway; therefore, Trim38 may be a promising target for treating cardiac hypertrophy.

Correspondence to: Dr Li Jiang, Institute of Cardiovascular Diseases, Tongren Hospital, Shanghai Jiao Tong University School of Medicine, 1111 Xianxia Road, Shanghai 200336, P.R. China
E-mail: jiangli@shtrhospital.com

Dr Lei Hou, Department of Cardiology, Songjiang Hospital Affiliated to Shanghai Jiaotong University School of Medicine, 746 Zhongshanzhong Road, Shanghai 201600, P.R. China
E-mail: dr_houlei@163.com

*Contributed equally

Abbreviations: HF, heart failure; Trim, tripartite motif; NAFLD, nonalcoholic fatty liver disease; MYH7, myosin heavy chain 7; ANP, atrial natriuretic peptide; TAC, transverse aortic constriction; PE, phenylephrine; KO, knockout; WT, wild-type; KEGG, Kyoto Encyclopedia of Genes and Genomes; GO, Gene Ontology; PTMs, post-translational modifications; SCF, Skp1/cullin/F box proteins; H&E, hematoxylin and eosin; PSR, picro-sirius red

Key words: pathological cardiac hypertrophy, Trim38, TAK1, JNK/P38 signaling pathway

Introduction

Heart failure (HF) is an end-stage cardiovascular disease, which has become a notable public health burden due to its high morbidity and mortality rates (1,2). Pathological cardiac hypertrophy is an early characteristic of HF, which manifests as the enlargement of cardiomyocytes, increased protein synthesis, reactivation of fetal genes and cardiac fibrosis (3). Notably, there is a lack of effective treatments for the management of pathological cardiac hypertrophy in clinical practice (4). Investigating the molecular mechanisms involved in the progression of cardiac hypertrophy may provide novel therapeutic targets for treating HF.

Tripartite motif (Trim) proteins are a group of proteins belonging to the E3 ubiquitin ligase family; these proteins are involved in the post-translational modification of proteins by catalyzing the binding of ubiquitin to its substrate (5). Trim38 is a prototypical Trim protein that is widely expressed in various cells, which contains a RING domain, two B-box domains, a coiled-coil domain and a PRY-SPRY domain, and

can be activated by type I IFNs and viral infection (6). Previous studies have shown that Trim38 serves critical regulatory roles in innate immune and inflammatory pathways, such as the Toll-like receptor signaling pathway, GAS/STING pathway, and MDA5- and RIG-I mediated antiviral response (7,8). Recently, it has been reported that Trim38 can attenuate cardiac fibrosis after myocardial infarction by suppressing TAK1 activation (9). Trim38 has also been shown to mitigate the development of non-alcoholic fatty liver disease (NAFLD) by promoting TAB2 degradation and inhibiting the MAPK signaling pathway (10). However, the role of Trim38 in pathological cardiac hypertrophy has not yet been fully elucidated.

The present study assessed the expression levels of Trim38 in a model of pressure overload-induced cardiac hypertrophy and examined its role in this pathological process.

Materials and methods

Trim38 knockout (Trim38-KO) mice. Trim38-KO mice were generated using the clustered regularly interspaced short palindromic repeats (CRISPR)/CRISPR associated protein 9 (Cas9) system. The guide RNA (gRNA) was designed using an online tool (http://chopchop.cbu.uib.no/). The target site was located ~150 base pairs downstream of the start codon ATG on exon 1; the sequence of this region (5'-GCAATGTCAGCCCAAAAACA-3') disrupts the entire protein domain. The Trim38-specific gRNA was cloned into the pUC57-sgRNA vector (cat. no. 51132; Addgene, Inc.). The Cas9 expression vector pST1374-Cas9 (cat. no. 44758; Addgene, Inc.) and the *in vitro* transcribed Trim38-sgRNA were combined. This mixture was microinjected into single-cell C57BL/6 mouse embryos using the FemtoJet 5247 microinjection system (Eppendorf SE). The injected embryos were then transferred into three pseudopregnant female ICR mice (weight, 29-32 g; age, 8-9 weeks; Beijing Vital River Laboratory Animal Technology Co., Ltd.). All mice were housed in a specific pathogen-free environment where temperature (22±2˚C), humidity (50-55%) and light cycles (12-h light/dark cycle) were strictly regulated. In addition, the mice had *ad libitum* access to both food and water. After a gestation period of 19-21 days, the F0 generation mice were born. A total of 2 weeks postpartum, genomic DNA was extracted from tail snips to genotype the mice using the following primers: Trim38-check forward (F)1, 5'-TGGGCT CAGACTTTAGCACG-3'; Trim38-check reverse (R)1, 5'-TCT TCCCAATAACAGCGCCA-3'.

Animal model of cardiac hypertrophy. The male wild-type (WT) C57BL/6 mice (age, 8 weeks; weight, 27-30 g) used were purchased from Beijing Vital River Laboratory Animal Technology Co., Ltd. The WT mice and Trim38-KO mice were randomly assigned to four experimental groups ,with initial sample sizes determined to account for potential attrition during the modeling phase. The group allocations were as follows: WT Sham (15 mice), WT TAC (15 mice), Trim38-KO Sham (15 mice) and Trim38-KO TAC (20 mice). Animals were excluded if they either died during surgery or failed to meet the predefined model success criteria. After exclusions, a total of 10 mice per group were included in the final dataset. Both WT and Trim38-KO mice underwent either sham surgery or TAC surgery to induce pressure overload. The mice were bred in a specific pathogen-free grade animal laboratory. Housing conditions included no more than three mice per cage, with free access to water and food, a 12-h light cycle, room temperature maintained at 22±2˚C and humidity controlled at 50-55%. During the modeling process, anesthesia was induced via intraperitoneal injection of a 3% sodium pentobarbital solution at a dose of 50 mg/kg. Transverse aortic constriction (TAC) was adopted to induce cardiac hypertrophy (11). After anesthesia, a 27G needle was placed parallel to the aorta. Next, a needle holder was utilized to pass a 7-0 suture through the aorta and ligate it together with the needle around the aorta. Once the ligation was complete, the needle was rapidly removed to establish aortic stenosis. The sham group underwent thoracotomy without aortic ligation.

Histological analysis. Upon completion of the experimental period, mouse hearts were harvested for analysis. The 8-week-old male C57BL/6 mice were euthanized via intraperitoneal injection of pentobarbital sodium (150 mg/kg body weight) to ensure a rapid and painless death. To confirm irreversible cessation of vital functions, the following criteria were monitored: i) Cessation of cardiac activity, verified by both thoracic palpation and direct visual inspection post-thoracotomy; ii) bilateral pupillary dilation under bright light examination; iii) absence of nociceptive reflexes, demonstrated by unresponsiveness to a standardized toe-pinch stimulus. Cardiac tissues were harvested only after confirmation of death. The heart tissues were fixed with 4% paraformaldehyde for 24 h and subsequently dehydrated through a graded series of ethanol prior to paraffin embedding. Specimens were sectioned at a thickness of 5 μm, and hematoxylin and eosin (H&E) staining was employed to assess cardiomyocyte size. For H&E staining, heart sections were incubated in hematoxylin working solution for 5 min followed by eosin solution for 3 min. In addition, picro-sirius red (PSR) staining was utilized to evaluate the extent of ventricular fibrosis. PSR staining involved applying a 1% PSR solution to the sections and staining them in a humidified chamber for 90 min. All procedures were conducted at room temperature (20-25˚C). H&E-stained sections were observed under a standard light microscope, whereas PSR-stained sections were examined under a polarized light microscope to facilitate collagen fiber visualization. Images were captured at x400 magnification and data were analyzed using the imaging analysis system Image-Pro Plus 6.0 (Media Cybernetics, Inc.).

Cell culture. Following surface sterilization through immersion in a 75% ethanol solution, 30 neonatal Sprague-Dawley rats (age, 1-3 days; SPF Biotechnology Co., Ltd.), were euthanized via decapitation using large, sterile straight scissors. Neonatal rat cardiomyocytes (NRCMs) were isolated from neonatal rats according to previously established methods (12). Specifically, the hearts of neonatal rats were excised, followed by removal of the atria while retaining the ventricles. NRCMs were subsequently harvested after treatment with 0.03% pancreatin and 0.04% type II collagenase. The digestion process with pancreatin and collagenase was conducted at 37˚C to maintain enzymatic activity. The initial digestion cycle lasted for 15 min, followed by subsequent digestion

cycles each lasting 10 min; three cycles were performed until complete tissue dissociation was achieved. Fibroblasts were eliminated using differential adhesion. The AC16 human cardiomyocyte cell line (cat. no. CC-Y1760) was obtained from Shanghai EK-Bioscience Biotechnology Co., Ltd. Both NRCMs and AC16 cells were seeded into 6-well plates at a density of $2x10^5$ cells/well and cultured in DMEM/F12 (cat. no. 10565018) supplemented with 10% fetal bovine serum (cat. no. 10099141C) and 100 U/ml penicillin/streptomycin (cat. no. 15140122) (all from Gibco; Thermo Fisher Scientific, Inc.) for 48 h under standard conditions (37˚C, 5% CO_2).

Recombinant vector construction. The Trim38-knockdown adenovirus was generated by constructing a replication-deficient adenovirus vector carrying short hairpin RNA (shRNA) targeting Trim38 (AdshTrim38), with the AdshRNA adenovirus containing a non-specific shRNA used as the control. The non-specific shRNA does not target any endogenous genes, thereby eliminating the potential for non-specific gene knockdown to interfere with experimental outcomes. Additionally, a rat adenovirus overexpressing Flag-Trim38 (AdTrim38) and an adenovirus containing dominant-negative TAK1 (Ad-dnTAK1) were constructed, with an empty vector (AdVector) used as the control. The dnTAK1 mutant effectively inhibits the normal activation of endogenous WT TAK1. The plasmid backbone used for these constructs was pAd-CMV (Thermo Fisher Scientific, Inc.) and 293 cells (American Type Culture Collection) were used as the packaging cell line for adenoviral production. Cells were transfected with 10 μg adenoviral plasmid using polyethyleneimine (PEI; cat. no. 24765-100; Polysciences, Inc.) at a DNA:PEI mass ratio of 1:3. The DNA-PEI complex was formed in serum-free medium (~22˚C, 15 min) and added to cells. After 6 h, the medium was replaced with fresh complete medium. Cells were cultured (37˚C, 5% CO_2) and observations began on day 2 post-infection at a consistent time point. Cytopathic effect (CPE) was assessed daily using an inverted microscope, with cell rounding, detachment and vacuolation recorded as key markers. CPE typically appeared within 5-7 days. For primary virus (P1) harvest, when 50-60% of cells exhibited CPE, both the cells and supernatant were collected. The mixture was centrifuged at 800 x g for 10 min at 4˚C, after which the supernatant was resuspended. The cell suspension was then subjected to three freeze-thaw cycles (liquid nitrogen/37˚C water bath) to release viral particles. The primary viral stock (P1 generation) harvested from the initial transfection of 293 cells was used to infect fresh 293 cells. Subsequent passages (P2-P4) were generated by repeating the harvest protocol under identical CPE progression criteria (50% cellular pathology). All viral generations were processed through identical centrifugation and freeze-thaw cycles as described for P1. Following three freeze-thaw cycles to lyse the cells, the lysate was clarified by centrifugation at 800 x g for 10 min at 4˚C, and the resulting supernatant was layered onto a discontinuous CsCl gradient (1.1, 1.3 and 1.4 g/ml) and ultracentrifuged (115,700 x g, 4˚C, 2 h; TH641 rotor; Thermo Fisher Scientific, Inc.). The viral band (between the 1.3 and 1.4 g/ml CsCl layers) was collected, dialyzed (4˚C, PBS + 5% glycerol), filtered (0.22 μm) and stored at -80˚C.

Adenoviruses were used to infect NRCMs at a multiplicity of infection (MOI) of 50 particles/cells for 24 h at 37˚C followed by detection and identification. The shRNA sequence targeting Trim38 was: 5'-GCACAAAGGTCA TACCTTATT-3'. The sequences used for the construction of the aforementioned adenoviral vectors were as follows: AdshTrim38-rat-F, CCGGTAGCTCTGTCTAAA GGTGGAACTCGAGTTCCACCTTTAGACAGAGCTATT TTTG, AdshTrim38-rat-R, AATTCAAAAAGCACAAAG GTCATACCTTATTCTCGAGAATAAGGTATGACCTTT GTGC; AdTrim38-rat-F, AGGCTAGCGATATCGGATCCA TGGGCTCAGACTTTAGCACAGTG, AdTrim38-rat-R, TCGTCCTTGTAATCACTAGTCTTCTTTCCATGATTAT TTATGGCAGGAGGGA; Ad-dnTAK1-mouse-F, GATGTC GCTATTAACCAGATAGAAAGTG; Ad-dnTAK1-mouse-R, CACTTTCTATCTGGTTAATAGCGACATC.

Plasmid construction. The Trim38 gene was amplified utilizing PCR. Subsequently, it was cloned into the GL107 vector [pSLenti-EF1-EGFP-P2A-Puro-CMV-MCS-3xFLAG-WPRE; OBiO Technology (Shanghai) Corp., Ltd.] using Seamless Cloning Kit [cat. no. SCNP-20/50; OBiO Technology (Shanghai) Corp., Ltd.]. This process generated a Trim38 overexpression plasmid designed to induce the stable overexpression of Trim38 in the AC16 cardiomyocyte cell line. The forward sequencing primer (CMV-F) was 5'-CGCAAATGGGCGGTAGGCGTG-3' and the reverse sequencing primer (101-R) was 5'-AGAGACAGC AACCAGGAT-3'.

Transduction and transfection. NRCMs were infected with the corresponding adenoviruses as aforementioned. AC16 cardiomyocytes were transfected with Trim38 overexpression plasmid to overexpress Trim38 using Fugene transfection reagent (cat. no. E2311; Promega Corporation), whereas the control group was transfected with an empty plasmid. Briefly, 2 μg plasmid DNA was used per well in a 6-well plate. The complex (plasmid DNA-Fugene HD mixture) was formulated at ~22˚C and transfection was performed at 37˚C. The complex was incubated with the cells for 48 h under standard conditions (37˚C, 5% CO_2) to facilitate transfection and DNA expression. Subsequently, the medium was replaced with serum-free DMEM/F12 for 12 h. Thereafter, phenylephrine (PE; 50 μM; cat. no. P6126; MilliporeSigma) was used to establish a cardiomyocyte hypertrophy model at 37˚C for 48 h. The control group was treated with an equivalent volume of PBS under the same conditions.

Immunofluorescence. NRCMs employed in the experiment were first fixed with 3.7% formaldehyde at room temperature for 15 min and permeabilized with 0.1% Triton X-100 for 20 min. After washing with PBS, the cells were blocked with 8% BSA (cat. no. A1933; MilliporeSigma) at room temperature for 60 min. A primary antibody against α-actinin (1:100; cat. no. 05-384; MilliporeSigma) was then applied and incubated overnight at 4˚C. After removing the primary antibody, a Alexa Fluor 488-conjugated secondary antibody [donkey anti-mouse IgG (H+L); 1:200; cat. no. A21202; Invitrogen; Thermo Fisher Scientific, Inc.] was added and incubated in the dark at 37˚C for 60 min. The cells were counterstained with SlowFade Gold antifade reagent containing DAPI for nuclear

staining, and cured at room temperature in the dark for 24 h. Alternatively, the cell samples were prepared as aforementioned and stained overnight at 4˚C with Actin-Tracker Red (1:100; cat. no. C2205S; Beyotime Institute of Biotechnology). The following day, the samples were directly mounted with DAPI and observed. Fluorescence images were acquired using a confocal laser scanning microscope (TCS SP8; Leica Microsystems GmbH). Image-Pro Plus 6.0 software was employed to measure the cell surface area.

Reverse transcription-quantitative PCR (RT-qPCR). RNA was isolated from mouse heart tissue or NRCMs using TRIzol® reagent (Invitrogen; Thermo Fisher Scientific, Inc.) and cDNA synthesis was carried out through RT of the RNA according to the manufacturer's protocol (cat. no. 04896866001; Roche Diagnostics). qPCR was performed to measure the expression levels of the selected genes, utilizing a specific qPCR kit (cat. no. 4913850001; Roche Diagnostics), with GAPDH used as an internal control. Primer details are provided in Table SI. The thermal cycling conditions were as follows: Pre-incubation at 95˚C for 10 min; followed by 40 cycles of amplification at 95˚C for 10 sec, 60˚ for 30 sec, 72˚C for 20 sec; melt curve at 95˚C for 5 sec, 60˚ for 1 min, 95˚C for 15 sec; and cooling at 40˚C for 10 sec. Based on the obtained crossing point values, relative quantification analysis was conducted using the $2^{-\Delta\Delta Cq}$ method (13).

Western blot analysis. Total protein was extracted from heart tissues or cardiomyocytes using RIPA lysis buffer (100 mg SDS, 29.2 mg EDTA, 788.2 mg Tris-HCl, 200 mg sodium deoxycholate, 1 ml NP-40 and 876.6 mg NaCl dissolved in double-distilled water; pH 7.5; final volume, 100 ml). Protein concentration was determined using a BCA assay kit. Subsequently, proteins (50 μg) were separated by SDS-PAGE on a 10% gel and were transferred to PVDF membranes. After blocking with 5% non-fat milk at room temperature for 1 h, the membranes were incubated with primary antibodies at 4˚C overnight. The following day, appropriate secondary antibodies were added and incubated for 1 h at room temperature in the dark. Immunoblots were visualized using the Odyssey Imaging System (LI-COR Biosciences) and the results were normalized to GAPDH levels as the internal control. Protein expression was semi-quantified using Image Lab 5.1 software (Bio-Rad Laboratories, Inc.). Detailed information regarding the antibodies is provided in Table SII.

Ubiquitination assays. AC16 cells transfected with the Trim38 overexpression plasmid and empty plasmid were lysed using a lysis buffer added at four times the volume (8 M urea, 1% protease inhibitor, 50 μM PR-619). The cells were sonicated in a 4˚C water bath for a total duration of 3 min using a high-intensity ultrasonic processor (Scientz) with the following parameters: 3-sec pulses followed by a 5-sec pause; power output, 220 W; frequency range, 20-25 kHz. The supernatant was collected and the protein concentration was determined using a BCA kit (cat. no. P0011; Beyotime Institute of Biotechnology) according to the manufacturer's instructions. Subsequently, the lysate was precipitated with 20% TCA, centrifuged at 4,500 x g for 5 min at 4˚C and washed with acetone. After air-drying, TEAB (200 μM) was added to the precipitate and dispersed by ultrasound. Trypsin was added at a ratio of 1:50 (enzyme to protein, w/w) and the mixture was digested overnight. The next day, trypsin was added at a ratio of 1:100 for a second digestion lasting 4 h. The solution was reduced with dithiothreitol (5 mM) and alkylated with iodoacetamide (11 mM) in the dark. To enrich the modified peptides, the peptides dissolved in NETN buffer (100 mM NaCl, 1 mM EDTA, 50 mM Tris-HCl, 0.5% NP-40, pH 8.0). Each sample was incubated with 40 μl pre-washed anti-diglycyl-lysine antibody conjugated agarose beads (cat. no. PTM1104; PTM Biolabs Inc.) at 4˚C overnight. Subsequently, the beads were washed four times with immunoprecipitation buffer solution (PTM Biolabs Inc.) and twice with deionized water. Bound peptides were subsequently eluted through two consecutive washes with 0.1% trifluoroacetic acid (100 μl per wash; pH ~2) while subjected to vigorous vortexing. The eluates were then combined and vacuum-dried. The resulting peptides were desalted with C18 ZipTips (MilliporeSigma).

Liquid chromatography-tandem mass spectrometry (LC-MS/MS) analysis. The peptides were dissolved in solvent A (0.1% formic acid and 2% acetonitrile in water) and loaded onto a homemade reversed-phase analytical column (length, 25 cm; internal diameter, 100 μm). The mobile phase consisted of solvent A and solvent B (0.1% formic acid in acetonitrile). Peptides were separated using following gradient; 0-40 min, 6-22% solvent B; 40-52 min, 22-30% B; 52-56 min, 30-80% solvent B; 56-60 min, 80% solvent B. All procedures were conducted at a constant flow rate of 450 nl/min on a NanoElute UHPLC system (Bruker Daltonics; Bruker Corporation).

Subsequently, the peptides were electrosprayed through a capillary source , generating charged droplets that underwent desolvation via solvent evaporation to yield gaseous ions. These ions were then analyzed in the timsTOF Pro2 mass spectrometry (Bruker Daltonics; Bruker Corporation). The electrospray voltage was set to 1.5 kV. Precursors and fragments were analyzed at the TOF detector, with a MS/MS scan range from 100-1,700 m/z. The timsTOF Pro2 was operated in parallel accumulation serial fragmentation (PASEF) mode. Precursors with charge states 0-5 were selected for fragmentation, and 10 PASEF-MS/MS scans were acquired per cycle. The dynamic exclusion was set to 24 sec. The resulting MS/MS data were processed using MaxQuant search engine (v.1.6.15.0; https://www.maxquant.org/maxquant/) (14). Tandem mass spectra were searched against the human SwissProt database (https://www.uniprot.org/) (15) concatenated with reverse decoy and contaminants database. Trypsin/P was specified as cleavage enzyme allowing up to 4 missing cleavages. Minimum peptide length was set at 7 and maximum number of modifications per peptide was set at 5. The mass tolerance for precursor ions was set at 20 ppm in the first search and 20 ppm in the main search, and the mass tolerance for fragment ions was set at 20 ppm. Due to sample pre-treatment with reduction and alkylation, carbamidomethyl modification on cysteine residues was set as a fixed modification; ubiquitylation on lysine residues was specified as a variable modification to identify ubiquitination sites. The false discovery rate of protein, peptide and peptide-spectrum match was adjusted to <1%.

Functional enrichment-based cluster analysis. Hierarchical clustering was conducted to classify differentially expressed proteins in the Trim38 overexpression group compared with the control group based on their function. Based on their expression levels, differentially expressed proteins were divided into four groups, namely Q1 to Q4, with Q4 representing the most significantly altered proteins. Gene Ontology (GO) classification and Kyoto Encyclopedia of Genes and Genomes (KEGG) pathway enrichment analyses were both conducted on each of the Q groups. GO annotation was accomplished by analyzing the identified proteins with eggnog-mapper software v2.0 (https://github.com/eggnogdb/eggnog-mapper) (16) and the KEGG database (https://www.genome.jp/kegg/) (17) was used to conduct KEGG pathway enrichment analysis. The Fisher's exact test was employed to analyze the significance of KEGG pathway enrichment of differentially expressed proteins. $P<0.05$ was considered to indicate a statistically significant difference.

Statistical analysis. All values are presented as the mean ± standard error of the mean. Normality was assessed using the Shapiro-Wilk test. For normally distributed data, comparisons between two groups were conducted using an unpaired two-tailed Student's t-test and one-way ANOVA was employed to evaluate differences among multiple groups. Post-hoc analysis was performed using Bonferroni correction for data with equal variances and Tamhane's T2 test for data with unequal variances. For data sets with skewed distributions, non-parametric statistical methods were applied: The Mann-Whitney U test for comparisons between two groups and the Kruskal-Wallis test followed by Dunn's post-hoc test for multiple comparisons. $P<0.05$ was considered to indicate a statistically significant difference.

Results

Trim38 expression is decreased in hypertrophic myocardial tissues and cardiomyocytes. A TAC-induced mouse model of cardiac hypertrophy was first established and the expression of Trim38 was detected using western blotting. As shown in Fig. 1A, the expression levels of Trim38 were gradually decreased after TAC, while the expression levels of biomarkers of cardiac hypertrophy, such as myosin heavy chain 7 (MYH7) and atrial natriuretic peptide (ANP), were increased. In addition, *in vitro* experiments confirmed the reduced expression of Trim38 in cardiomyocytes stimulated with PE. After 24 h of treatment with PE, NRCMs displayed an altered morphology, indicating hypertrophy, which was more pronounced after 48 h of PE treatment (Fig. 1B). Western blot analysis (Fig. 1C) also demonstrated a decrease in Trim38 expression in NRCMs treated with PE, alongside increased levels of MYH7 and ANP, further confirming the development of hypertrophy in the cells. Therefore, Trim38 may be considered a potential target for cardiac hypertrophy.

Loss of Trim38 aggravates cardiac hypertrophy. Trim38-KO mice were produced and Trim38 expression was validated using western blotting to investigate whether Trim38 contributes to cardiac hypertrophy (Fig. 2A). At the baseline, there were no significant differences in heart weight, myocardial hypertrophy and myocardial fibrosis levels between WT sham mice and Trim38-KO sham mice (Figs. 2B-F, and S1A and B). These findings suggested that Trim38-KO had no significant impact on myocardial hypertrophy and myocardial fibrosis under physiological conditions. However, compared with in WT mice, heart weight, heart weight/body weight ratio and heart weight/tibia length ratio were increased in Trim38-KO mice 4 weeks after TAC (Fig. 2B). In addition, histological analysis of cardiac tissue sections demonstrated a marked increase in cardiomyocyte size upon H&E staining in the Trim38-KO TAC group compared with in the WT TAC group (Fig. 2C). Furthermore, PSR staining revealed that Trim38-KO significantly aggravated myocardial fibrosis (Fig. 2D). Molecular analyses, including qPCR and western blotting, confirmed that Trim38-KO led to elevated mRNA and protein expression levels of ANP, brain natriuretic peptide (BNP) and MYH7 in the heart (Fig. 2E and G). Additionally, Trim38-KO upregulated the expression of fibrosis markers, including collagen type I α1 (collagen Ia), collagen III and connective tissue growth factor (CTGF) following TAC (Fig. 2F and H). Taken together, these findings suggested that Trim38-KO may contribute to the development of cardiac hypertrophy.

Trim38 ameliorates PE-induced cardiomyocyte hypertrophy. The present study also investigated the role of Trim38 in cardiomyocytes *in vitro*. AdshTrim38 infection was used to downregulate Trim38 expression in NRCMs, while AdFlag-Trim38 infection was used to overexpress Trim38 (Fig. 3A). After treatment with PE for 48 h, cells with Trim38 knockdown were of a larger size, and exhibited enhanced expression levels of ANP and BNP, compared with in cells infected with AdshRNA (Figs. 3B and D, and S1C). By contrast, Trim38 overexpression inhibited cardiomyocyte hypertrophy, and downregulated PE-induced expression levels of ANP and BNP (Figs. 3C and E, and S1D). Thus, these findings demonstrated that Trim38 could protect against cardiomyocyte hypertrophy *in vitro*.

Trim38 protects against cardiac hypertrophy via the TAK1/JNK/P38 signaling pathway. Given that Trim38 is an E3 ubiquitin ligase, ubiquitinomics analysis was conducted on cardiomyocytes overexpressing Trim38 treated with PE to explore how Trim38 regulates cardiac hypertrophy. A heat map demonstrating differences in protein expression between the Trim38 overexpression group and the control group is shown in Fig. 4A. Using cluster analysis, differentially modified proteins were divided into four groups (Q1, Q2, Q3 and Q4). GO enrichment analyses indicated that they were involved in 'regulation of protein phosphorylation' (Fig. 4B). KEGG analysis indicated that differentially modified proteins in the Q3 group (with fold changes ranging from 1.5 to 2) were enriched in the 'MAPK signaling pathway' (Fig. 4C). Therefore, further studies placed a particular emphasis on phosphorylation of the MAPK signaling pathway. Western blotting was conducted to identify potential proteins involved in the MAPK signaling pathway, and it was unveiled that after TAC, TAK1 phosphorylation was markedly upregulated in Trim38-KO mice compared with in the WT TAC group (Fig. 5A-C). In addition, Trim38-KO TAC mice exhibited a significant increase in the phosphorylation of JNK and P38 during cardiac hypertrophy compared with

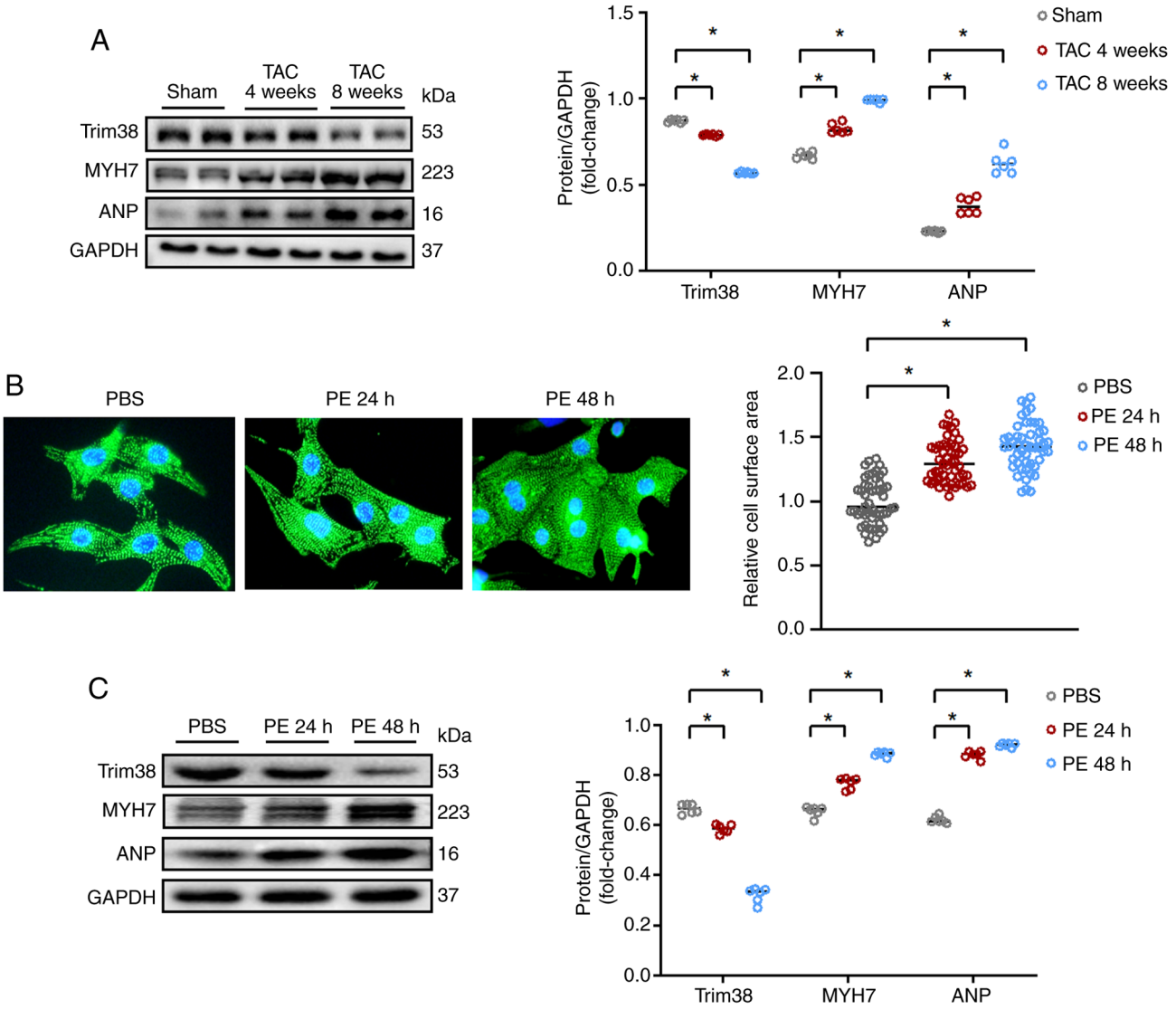

Figure 1. Trim38 expression is decreased in cardiac hypertrophy. (A) Western blotting was conducted to assess the expression levels of Trim38, MYH7 and ANP in heart tissues from mice under pressure overload (n=6). (B) Microscopic images of NRCMs stimulated with PE (x40 magnification). (C) Trim38, MYH7 and ANP expression levels were detected using western blot analysis in hypertrophic NRCMs induced by PE. Blots represent one of six replicated experiments. *P<0.05. ANP, atrial natriuretic peptide; MYH7, myosin heavy chain 7; NRCMs, neonatal rat cardiomyocytes; PE, phenylephrine; TAC, transverse aortic constriction; Trim38, tripartite motif 38.

WT TAC mice (Fig. 5D-F). Subsequently, *in vitro* experiments were conducted to confirm the underlying mechanism. Western blotting showed that Trim38 knockdown enhanced the phosphorylation of TAK1, JNK and P38, whereas Trim38 overexpression inhibited the phosphorylation of TAK1, JNK and P38 in NRCMs treated with PE (Fig. 6A-C). Overall, these results preliminarily indicated that Trim38 inhibited activation of the MAPK pathway in cardiac hypertrophy.

Blocking the activity of TAK1 ameliorates Trim38 knockdown-induced cardiomyocyte hypertrophy. Ad-dnTAK1 was generated, which lacks kinase activity, to function as a TAK1 inhibitor. This allowed for investigation as to whether Trim38 modulates cardiac hypertrophy via the TAK1/JNK/P38 signaling pathway. The dnTAK1 harbors a dominant-negative mutation that abolishes its kinase activity and effectively neutralizes the function of WT TAK1. Upon infection with Ad-dnTAK1, this mutant form effectively neutralizes the activity of WT TAK1 while maintaining its own kinase-inactive state.

Ad-dnTAK1 was co-transfected into NRCMs with either AdshRNA or AdshTrim38, and the following observations were made. Under PBS conditions, compared with in cells infected with AdshRNA, the expression levels of TAK1 were increased in cells co-transfected with Ad-dnTAK1 and AdshRNA (Ad-dnTAK1 + AdshRNA), whereas the expression levels of p-TAK1 remained unchanged (Fig. S2A). Similarly, the cell area was not significantly altered between these two groups (Fig. S2B). These findings suggested that, despite the increased expression levels of TAK1, its biological activity remained unaltered at baseline due to the dominant-negative effect of Ad-dnTAK1; this prevents the phosphorylation of TAK1 and any resultant phenotypic alterations in the cells.

Upon treatment with PE, consistent with the aforementioned findings, Trim38 knockdown in NRCMs resulted in increased TAK1 phosphorylation (Fig. 7A) accompanied by

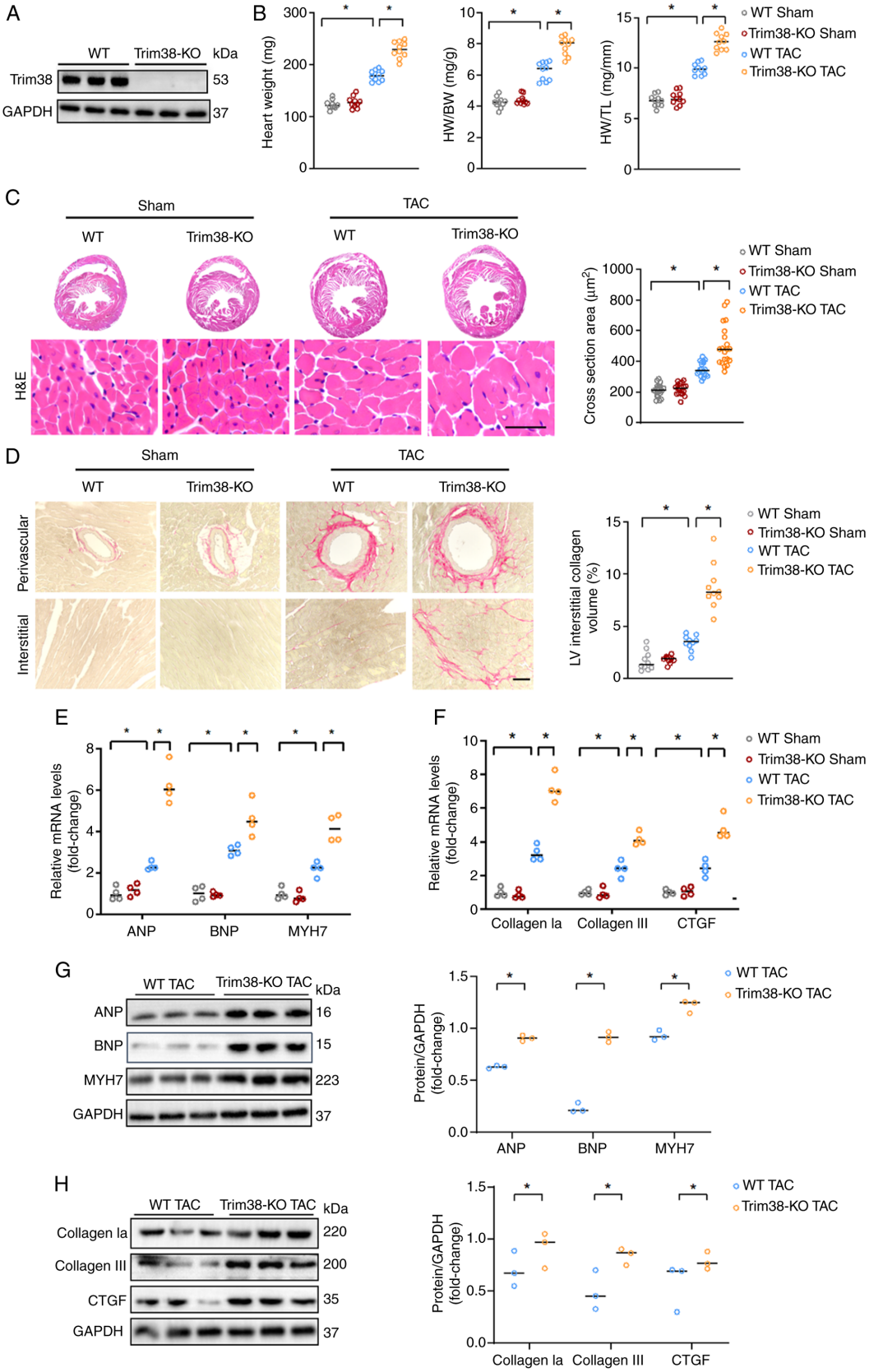

Figure 2. Trim38-KO exacerbates cardiac hypertrophy. (A) Trim38 expression levels in Trim38-KO mice were detected using western blot analysis. (B) HW, HW/BW ratio and HW/TL ratio of WT and Trim38-KO mice subjected to TAC (n=10). (C) H&E staining of heart tissue sections from WT mice and Trim38-KO mice (scale bars, 25 μm). Cell section area was quantified in each group (n>50 cells/group). (D) Picro-sirius red staining showing fibrosis of heart tissue sections from WT and Trim38-KO mice (scale bars, 50 μm). Collagen volume was quantified in each group (n>10 files/group). mRNA expression levels of (E) hypertrophic markers ANP, BNP and MYH7, and (F) collagen Ia, collagen III and CTGF in each group (n=4 independent experiments). Western blot analyses of the expression levels of (G) ANP, BNP and MYH7, and (H) collagen Ia, collagen III and CTGF in WT mice and Trim38-KO mice after TAC. Blots represent one of three replicated experiments. *P<0.05. ANP, atrial natriuretic peptide; BNP, brain natriuretic peptide; BW, brain weight; collagen Ia, collagen type I α1; CTGF, connective tissue growth factor; H&E, hematoxylin and eosin; HW, heart weight; KO, knockout; LV, left ventricle; MYH7, myosin heavy chain 7; TAC, transverse aortic constriction; TL, tibia length; Trim38, tripartite motif 38; WT, wild-type.

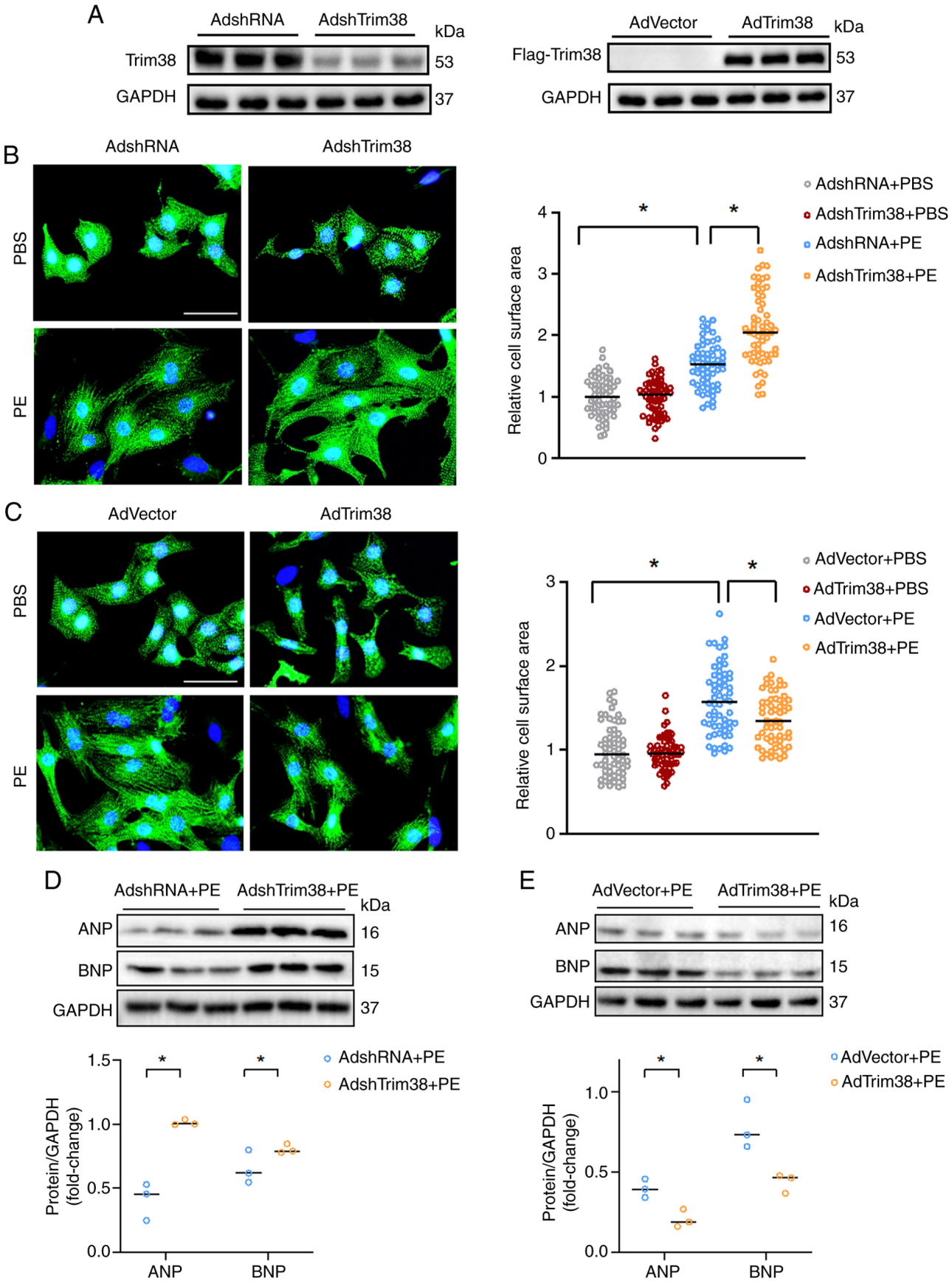

Figure 3. Trim38 ameliorates PE induced cardiomyocyte hypertrophy. (A) Western blot analysis of Trim38 expression in NRCMs infected with the indicated Ads. (B) Representative α-actinin staining of NRCMs infected with AdshRNA or AdshTrim38 treated with PBS or PE (scale bar, 20 μm). (C) Representative α-actinin staining of NRCMs infected with AdVector or AdTrim38 treated with PBS or PE (scale bar, 20 μm). Cell cross-sectional area was quantified for each group (n>50 cells/group). (D and E) Western blot analysis of hypertrophic markers ANP and BNP in NRCMs from each group treated with PE. *P<0.05. Blots represent one of three replicated experiments. Ad, adenovirus; ANP, atrial natriuretic peptide; BNP, brain natriuretic peptide; NRCMs, neonatal rat cardiomyocytes; PE, phenylephrine; sh, short hairpin; Trim38, tripartite motif 38.

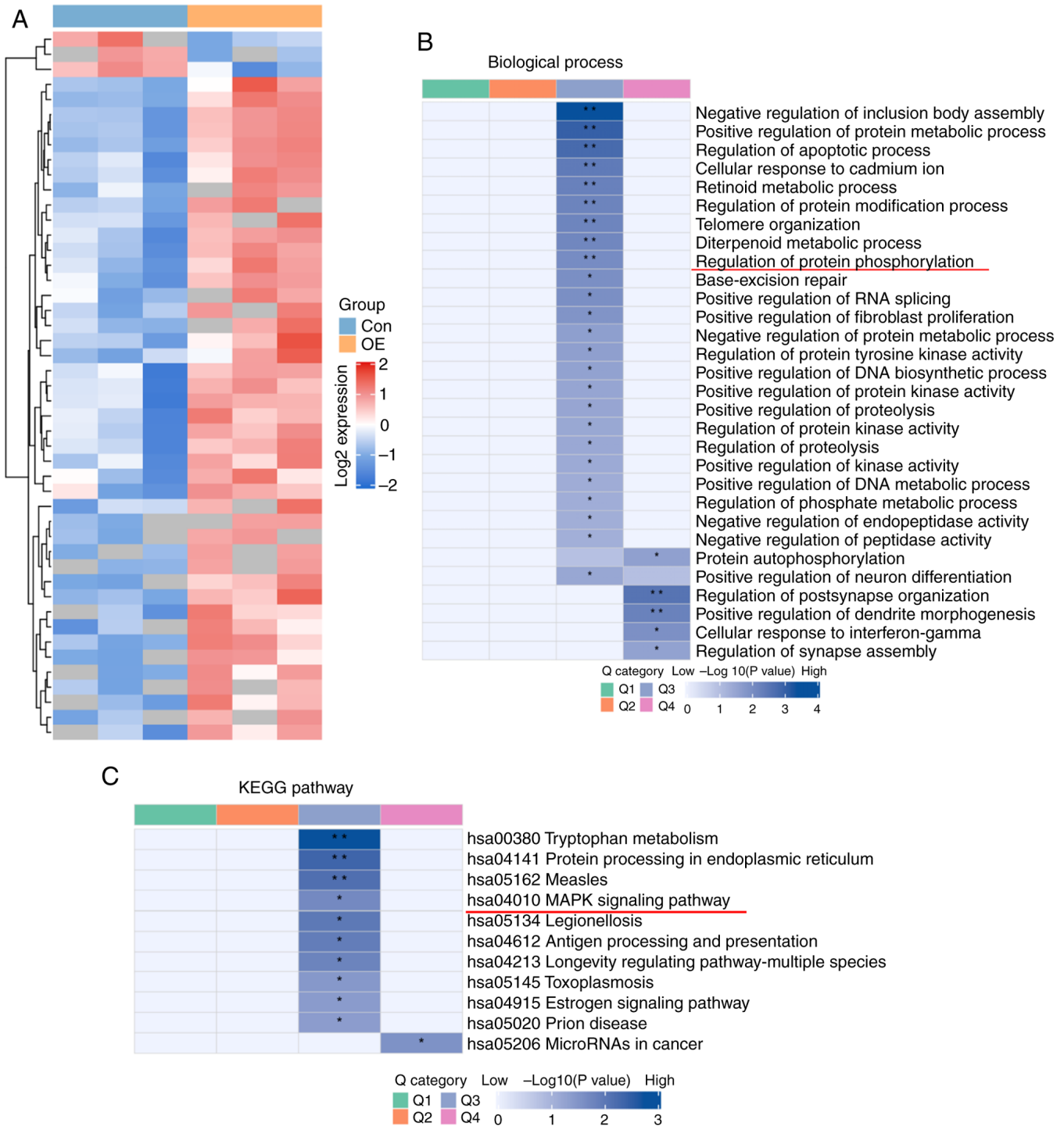

Figure 4. Ubiquitinomics analysis of cardiomyocyte overexpressing Trim38. (A) Heat map showing differentially expressed proteins identified between Trim38-OE cardiomyocytes and the control group in ubiquitinomics analysis. (B) Biological process analysis performed using the Gene Ontology database. (C) Protein pathway annotation obtained based on the KEGG pathway database. Significant functional enrichment of differentially expressed proteins is visualized by a gradient of blue blocks scaled to -log10(P-value) () *P<0.05, **P<0.01. OE, overexpression; KEGG, Kyoto Encyclopedia of Genes and Genomes; Trim38, tripartite motif 38.

an enlargement of cell area (Fig. 7B), and an upregulation of the hypertrophy markers ANP and BNP compared with in NRCMs infected with AdshRNA (Figs. 7C and S1F). Notably, co-infection with Ad-dnTAK1 and AdshRNA significantly suppressed TAK1 phosphorylation relative to AdshRNA alone. A parallel phenomenon was observed in AdshTrim38-infected cells: Co-infection with AdshTrim38 and Ad-dnTAK1 led to a significant reduction in TAK1 phosphorylation compared with infection with AdshTrim38 alone (Figs. 7A and S1E). Crucially, comparing the NRCMs co-infected with Ad-dnTAK1 and AdshTrim38 to those infected with Ad-shTrim38 alone revealed that blockade of TAK1 activity via Ad-dnTAK1 abrogated the pro-hypertrophic effects of Trim38 deficiency in cardiomyocytes (Figs. 7A-C and S1F). Collectively, these

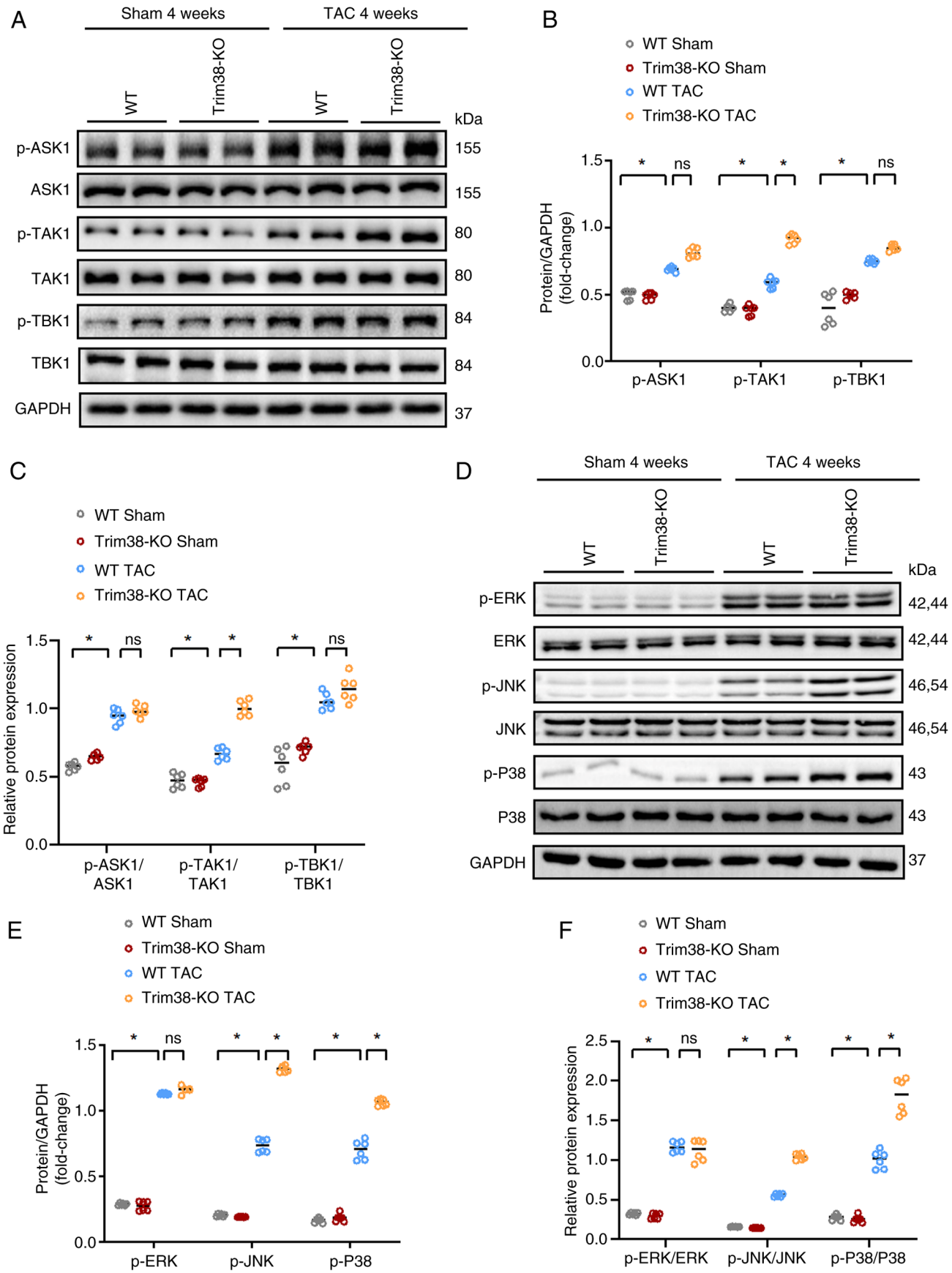

Figure 5. Trim38-KO leads to further activation of the MAPK signaling pathway in mice after TAC. (A) Western blot analysis comparing the total and p-levels of ASK1, TAK1 and TBK1 between Trim38-KO mice and WT mice. (B) Semi-quantification analysis of phosphorylation levels of ASK1, TAK1 and TBK1 in each group. (C) Ratios of p-/total protein levels for ASK1, TAK1 and TBK1 in each group. (D) Western blot analysis of the total and p-levels of ERK, JNK and P38 in Trim38-KO mice and WT mice. (E) Semi-quantification of the phosphorylation levels of ERK, JNK and P38 in hearts from Trim38-KO mice and WT mice. (F) p-ERK/total ERK, p-JNK/total JNK and p-P38/total P38 ratios in each group. Blots represent one of six replicated experiments. *P<0.05. ASK1, apoptosis signal-regulating kinase 1; KO, knockout; p-, phosphorylated; TAC, transverse aortic constriction; Trim38, tripartite motif 38; WT, wild-type.

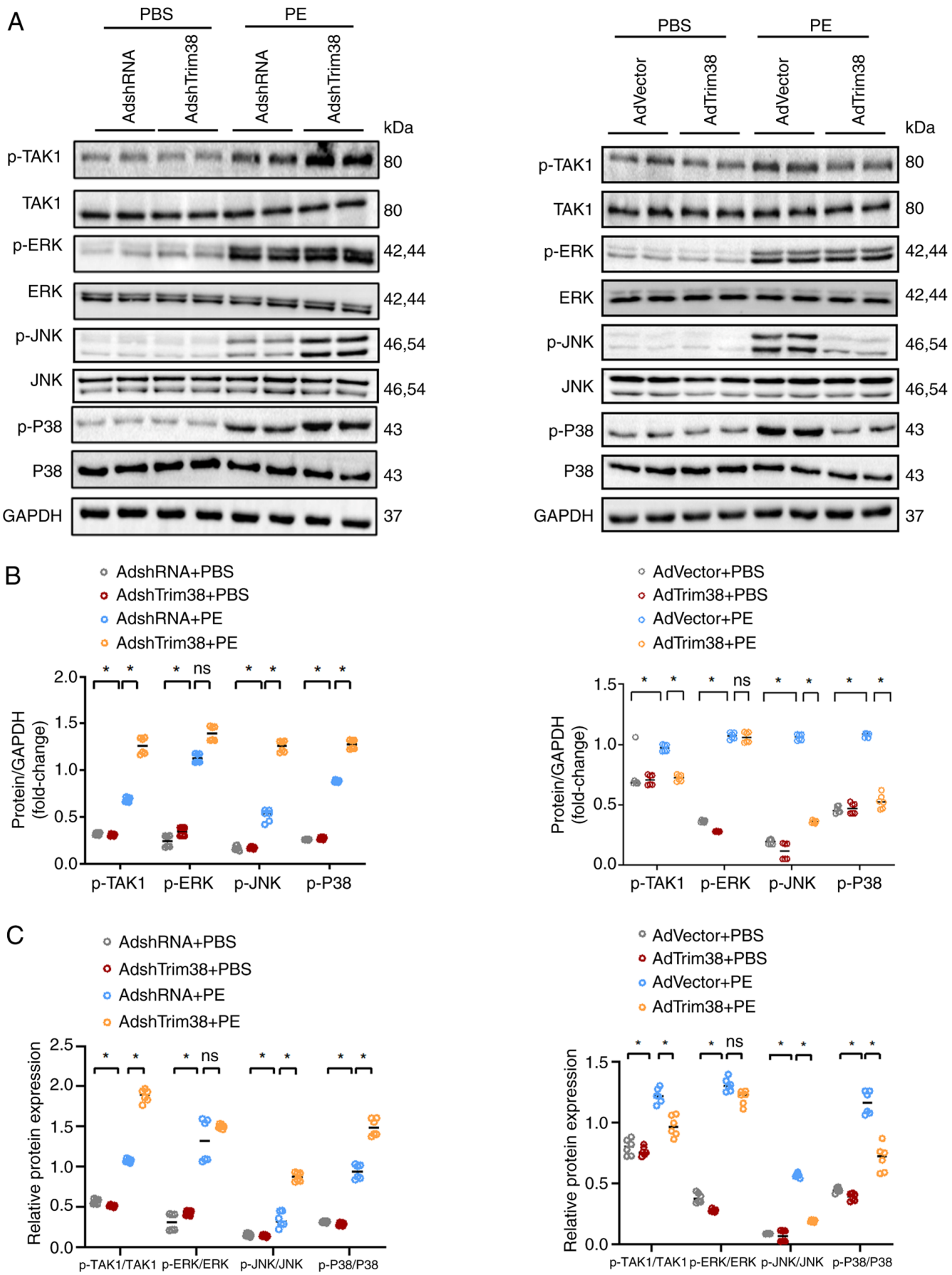

Figure 6. Trim38 suppresses the TAK1/JNK/P38 signaling pathway in NRCMs treated with PE. (A) Western blot analysis of MAPK signaling pathway-related proteins in NRCMs infected with AdshRNA and AdshTrim38, or AdVector and AdTrim38. (B) Semi-quantitative analysis of p-levels of MAPK signaling-related proteins in each group. (C) Ratios of p-/total protein levels for TAK1, ERK, JNK and P38 in each group. Blots represent one of six replicated experiments. *P<0.05. Ad, adenovirus; NRCMs, neonatal rat cardiomyocytes; p-, phosphorylated; PE, phenylephrine; sh, short hairpin; Trim38, tripartite motif 38.

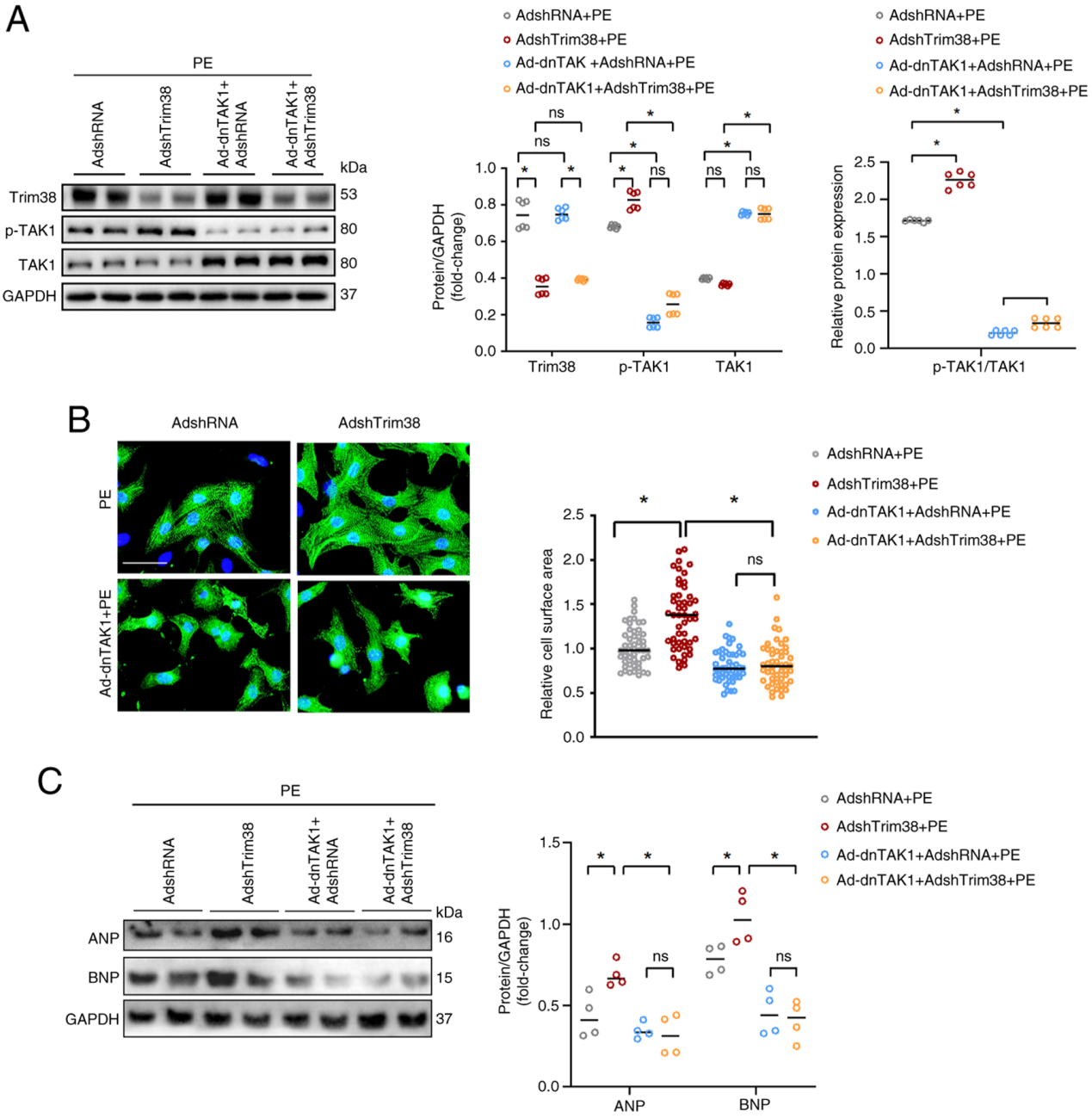

Figure 7. TAK1 is essential for Trim38-mediated improvement of cardiac hypertrophy. (A) Western blot analysis and semi-quantification of Trim38, TAK1 and p-TAK1 in neonatal rat cardiomyocytes infected with the indicated Ads and treated with PE. The p-TAK1/TAK1 ratio is also displayed. Blots represent one of six replicated experiments. (B) Representative images of α-actinin staining and quantification of cell cross-sectional area for each group (n>50 cells/group) (scale bar, 20 μm). (C) Western blot analysis and semi-quantitation of the expression levels of ANP and BNP in each group. Blots represent one of four replicated experiments. *P<0.05. Ad, adenovirus; ANP, atrial natriuretic peptide; BNP, brain natriuretic peptide; dnTAK1, dominant-negative TAK1; p-, phosphorylated; PE, phenylephrine; sh, short hairpin; Trim38, tripartite motif 38.

findings indicated that Trim38 alleviated cardiomyocyte hypertrophy in a manner that is dependent on TAK1 activity.

Discussion

A previous study revealed that Trim38 expression is significantly downregulated within the cardiac tissues of mice subjected to LAD coronary artery permanent ligation, a well-characterized model of acute myocardial infarction (AMI), and is also reduced in coronary blood samples from patients with AMI. Furthermore, this previous study demonstrated that suppression of Trim38 can enhance the proliferative and secretory activities of cardiac fibroblasts (CFs), thereby exacerbating cardiac fibrosis (9). Conversely, upregulation of Trim38 expression has been observed to mitigate these fibrotic responses, highlighting its protective role against cardiac fibrosis under ischemic conditions (9). The present study revealed that Trim38 confers protection against pathological myocardial hypertrophy in response to pressure overload. Initial observations demonstrated downregulated Trim38 expression in hypertrophic cardiomyocytes and cardiac tissues. To further investigate this phenomenon,

Trim38-KO mice were generated. Under physiological conditions, these mice exhibited no significant differences in cardiac structure or function compared with their WT counterparts; however, under conditions of pressure overload, Trim38-KO exacerbated pathological hypertrophy, as evidenced by increased heart weight, enlarged cardiomyocyte area in cardiac tissue sections and elevated expression of hypertrophy markers, such as MYH7, ANP and BNP, in Trim38-KO cardiac tissues. Consistent with these *in vivo* findings, parallel *in vitro* experiments demonstrated that Trim38 knockdown led to increased cardiomyocyte size and upregulation of hypertrophy markers, whereas Trim38 overexpression resulted in reduced cell size and downregulation of these markers under PE stimulation. Collectively, these findings confirmed that Trim38 may have a crucial role in modulating pathological hypertrophy. Specifically, Trim38 could attenuate cardiac hypertrophy through inhibition of the JNK/P38 signaling pathway. Mechanistic insights further revealed that regulation of TAK1 phosphorylation by Trim38 is a critical factor in this process. To the best of our knowledge, the present study is the first to provide evidence that Trim38 alleviates pressure overload-induced pathological hypertrophy by inhibiting the TAK1/JNK/P38 signaling pathway.

The development of cardiac hypertrophy is accompanied by adaptive changes in protein expression, which are regulated by various factors, including gene transcription, mRNA translation and post-translational modifications (PTMs) (18). PTMs increase the complexity and diversity of proteins by adding or introducing new functional groups (19). Ubiquitination is a common form of PTM and a reversible process in which ubiquitin binds to the amino acid side, or C-terminal or N-terminal of proteins. Through diverse modifications, specifically the structural variability of ubiquitin chains formed by distinct lysine linkages (e.g., K48, K63) or linear M1 linkages, and specific recognition mechanisms, ubiquitination can rapidly and flexibly regulate signaling pathways without relying on changes in gene expression or waiting for transcription and translation processes. The dynamic nature of ubiquitination may make it more efficient than transcriptional regulation, which requires the activation of gene expression and the synthesis of new proteins (20). Ubiquitination serves a crucial role in determining protein structure, localization and function, playing a complex and precise regulatory role in cardiac hypertrophy (21). Trim family proteins are involved in various processes associated with cardiac hypertrophy through their ubiquitin ligase activity. These proteins facilitate the ubiquitination and degradation of specific substrates, which directly impacts the signaling pathways and protein turnover associated with hypertrophic responses. Notably, Trim65 has been demonstrated to prevent pathological cardiac hypertrophy by promoting mitochondrial autophagy through the Jak1/Stat1 signaling pathway (22). Moreover, Trim44 has been reported to promote cardiac hypertrophy by upregulating the expression of NOX4 and enhancing ferroptosis (23). The present study observed a decreased expression of Trim38 in cardiac hypertrophy *in vivo* and *in vitro*. After TAC, Trim38-KO increased cell size, aggravated fibrosis, and upregulated the expression of hypertrophic and fibrosis markers. Consequently, these findings suggested that Trim38 serves a crucial role in alleviating pressure overload-induced cardiac hypertrophy.

Ubiquitination experiments were conducted to elucidate the underlying mechanisms of Trim38 in cardiac hypertrophy. Using KEGG and GO enrichment analyses, several key pathways were identified. Notably, the MAPK pathway emerged as a classical pathway associated with the progression of cardiac hypertrophy. It has previously been shown that Trim38 suppresses cardiac fibrosis by attenuating the TAK1/MAPK signaling pathway in CFs (9). Consequently, the present study focused on the MAPK signaling pathway and discovered that Trim38 can modulate phosphorylation within this pathway. Multiple PTMs have been reported to maintain cellular homeostasis (24), and the cooperation of ubiquitination with other forms of PTMs is crucial for the orchestration of biological activities. The interplay between ubiquitination and phosphorylation regulates cellular processes and has been extensively explored in previous studies (25-27). Skp1/cullin/F box proteins (SCF) have been well identified as ubiquitin ligases responsible for phosphorylation-mediated ubiquitination. The F-box domain of SCF recognizes and binds to phosphodegron motifs, leading to substrate polyubiquitination, which typically results in proteasomal degradation (28). In addition to direct interaction with phosphorylated substrates, Trim16 has been demonstrated to ubiquitinate both TAK1 and p-TAK1, and promote the proteasomal degradation of p-TAK1 in nonalcoholic steatohepatitis through K-48 ubiquitination (29).

The MAPK signaling pathway is a highly conserved pathway that facilitates the activation of numerous transcription factors. It is activated in the hypertrophic myocardial tissue of mice induced by PE or pressure overload and in diseased human hearts (30). TAK1 functions as an 'initiation switch' that activates the MAPK signaling pathway, and upregulation of TAK1 phosphorylation appears to be an adaptive mechanism after TAC. Cardiac-specific ablation of TAK1 in mice has been shown to predispose them to cardiac hypertrophy and HF (31). Furthermore, the results of the present study revealed that overexpression of Trim38 inhibited the phosphorylation of TAK1, while Trim38 knockdown upregulated p-TAK1 expression and activated the JNK/P38 signaling pathway. To determine whether Trim38 protects against cardiac hypertrophy via p-TAK1, dnTak1 was used to block TAK1 binding to TAB1, thereby inhibiting TAK1 activation (32). p-TAK1 inactivation reversed cell enlargement and inhibited the expression of hypertrophic markers induced by Trim38 knockdown *in vitro*. Taken together, these findings suggested that Trim38 may ameliorate cardiac hypertrophy by inhibiting TAK1 phosphorylation.

The interaction between Trim38 and TAK1 has been investigated in several studies. Mechanistically, TAK1 activation necessitates the binding of TAB1, TAB2 and TAB3 to form the TAK1-TAB complex (33). TAB1 triggers the phosphorylation of TAK1, whereas TAB2 links TAK1 to the upstream proteins. Moreover, TAB2 and TAB3 serve a crucial role in maintaining the activation of TAK1 (34). Notably, emerging evidence has highlighted Trim38 as a key modulator of the TAK1-TAB complex across diverse pathological contexts, suggesting its potential role in fine-tuning TAK1-mediated signaling cascades. Previous studies have indicated that Trim38 mediates lysosome-dependent degradation of TAB2, thereby inhibiting TAK1 and the NFκB signaling pathway *in vitro* (35,36). In CFs treated with PE, Trim38 overexpression

has been shown to inhibit total ubiquitination and K63-linked ubiquitination of TAK1, which seems to be inconsistent with the fact that Trim38 acts as an E3 ubiquitin ligase that can promote ubiquitination. Subsequent analysis in the same study unveiled that Trim38 can promote TAB2 degradation, resulting in reduced TAK1 ubiquitination and phosphorylation (9). A similar observation has been made in NAFLD; Trim38 overexpression has been shown to downregulate TAB2 expression, thereby inhibiting the phosphorylation of TAK1 and MAPK signaling pathways (10). The present study confirmed previous findings and contributed additional evidence that Trim38 can protect against cardiac hypertrophy by suppressing TAK1 phosphorylation and activating the JNK/P38 signaling pathway. Based on previous findings, it was hypothesized that the reduction in TAK1 phosphorylation may be attributed to increased Trim38-mediated degradation of TAB2. This phenomenon could subsequently disrupt the binding of TAK1 to its upstream adaptors. However, further studies are needed to fully understand the underlying mechanisms.

There are several limitations in the present study that warrant acknowledgment. Firstly, a notable limitation of the study is the lack of cardiac ultrasound data, which prevented a direct assessment of ventricular wall thickness and overall cardiac function. While histological and molecular analyses provide supportive evidence for cardiac hypertrophy, these methods cannot fully replicate the distinct advantages of cardiac ultrasound in evaluating cardiac structure and function. Future studies should incorporate cardiac ultrasound to offer a more comprehensive evaluation of cardiac function and myocardial hypertrophy-related pathological changes. Additionally, the current study did not provide conclusive evidence on the decrease of Trim38 in the blood of patients with HF. Based on RNA-sequencing data from the Human Protein Atlas (https://www.proteinatlas.org/ENSG00000111666-TRIM38)(37) and GeneCards (https://www.genecards.org/cgi-bin/carddisp.pl?gene=TRIM38) (38), Trim38 demonstrates low expression levels in whole blood (TPM <1). This suggests potentially low concentrations of TRIM38 in circulation, thereby presenting challenges for its detection. Moreover, further investigation is necessary to explore the specific mechanism underlying the interaction between Trim38 and TAK1 in cardiac hypertrophy. Finally, clinical studies are required to validate the association between Trim38 and pressure overload-induced cardiac hypertrophy.

In conclusion, the present study demonstrated that Trim38 serves a protective role against pressure overload-induced pathological cardiac hypertrophy by suppressing the TAK1/JNK/p38 signaling axis. By contrast, Trim38 deficiency exacerbated myocardial hypertrophy and upregulated hypertrophic biomarkers (ANP/BNP). Mechanistically, Trim38 deficiency may activate TAK1 phosphorylation and the downstream MAPK pathway. Conversely, its overexpression has been shown to inhibit TAK1 phosphorylation and downstream MAPK pathway activation. Crucially, the detrimental effects of Trim38 knockdown were revealed to be mitigated by TAK1 inhibition, identifying TAK1 as a central mediator of Trim38-mediated cardioprotection. To the best of our knowledge, the present study is the first to highlight Trim38 as a novel negative regulator of pathological cardiac remodeling, positioning it as a promising therapeutic target for combating heart failure.

Acknowledgements

Not applicable.

Funding

No funding was received.

Availability of data and materials

The mass spectrometry proteomics data have been deposited to the ProteomeXchange Consortium via the PRIDE partner repository with the dataset identifier PXD060763 or at the following URL: https://www.ebi.ac.uk/pride/archive/projects/PXD060763. The other data generated in the present study may be requested from the corresponding author.

Authors' contributions

LJ and LH conceived the study and provided financial support. YP, LW, JX, XX and CG performed the experiments, collected the data and prepared the figures. YP was a major contributor in writing the manuscript. YP and LW confirm the authenticity of all the raw data. All authors contributed to the article, and read and approved the final version of the manuscript.

Ethics approval and consent for participation

The animal study was reviewed and approved by Shanghai Tongren Hospital Ethics Committee (approval no. A2023-086-01; Shanghai, China).

Patient consent for publication

Not applicable.

Competing interests

The authors declare that they have no competing interests.

References

1. McDonagh TA, Metra M, Adamo M, Gardner RS, Baumbach A, Böhm M, Burri H, Butler J, Čelutkienė J, Chioncel O, *et al*: 2021 ESC guidelines for the diagnosis and treatment of acute and chronic heart failure. Eur Heart J 42: 3599-3726, 2021.
2. Levy D, Larson MG, Vasan RS, Kannel WB and Ho KK: The progression from hypertension to congestive heart failure. JAMA 275: 1557-1562, 1996.
3. Martin TG, Juarros MA and Leinwand LA: Regression of cardiac hypertrophy in health and disease: Mechanisms and therapeutic potential. Nat Rev Cardiol 20: 347-363, 2023.
4. Katz AM and Rolett EL: Heart failure: When form fails to follow function. Eur Heart J 37: 449-454, 2016.
5. Dikic I: Proteasomal and autophagic degradation systems. Annu Rev Biochem 86: 193-224, 2017.
6. Hu MM and Shu HB: Multifaceted roles of TRIM38 in innate immune and inflammatory responses. Cell Mol Immunol 14: 331-338, 2017.
7. Xue Q, Zhou Z, Lei X, Liu X, He B, Wang J and Hung T: TRIM38 negatively regulates TLR3-mediated IFN-β signaling by targeting TRIF for degradation. PLoS One 7: e46825, 2012.
8. Hu MM, Yang Q, Xie XQ, Liao CY, Lin H, Liu TT, Yin L and Shu HB: Sumoylation promotes the stability of the DNA sensor cGAS and the adaptor STING to regulate the kinetics of response to DNA virus. Immunity 45: 555-569, 2016

9. Lu Z, Hao C, Qian H, Zhao Y, Bo X, Yao Y, Ma G and Chen L: Tripartite motif 38 attenuates cardiac fibrosis after myocardial infarction by suppressing TAK1 activation via TAB2/3 degradation. iScience 25: 104780, 2022.
10. Yao X, Dong R, Hu S, Liu Z, Cui J, Hu F, Cheng X, Wang X, Ma T, Tian S, *et al*: Tripartite motif 38 alleviates the pathological process of NAFLD-NASH by promoting TAB2 degradation. J Lipid Res 64: 100382, 2023.
11. Pang Y, Ma M, Wang D, Li X and Jiang L: TANK promotes pressure overload induced cardiac hypertrophy *via* activating AKT signaling pathway. Front Cardiovasc Med 8: 687540, 2021.
12. Ehler E, Moore-Morris T and Lange S: Isolation and culture of neonatal mouse cardiomyocytes. J Vis Exp 6: 50154, 2013.
13. Livak KJ and Schmittgen TD: Analysis of relative gene expression data using real-time quantitative PCR and the 2(-Delta Delta C(T)) method. Methods 25: 402-408, 2001.
14. Cox J and Mann M: MaxQuant enables high peptide identification rates, individualized p.p.b.-range mass accuracies and proteome-wide protein quantification. Nat Biotechnol 26: 1367-1372, 2008.
15. UniProt Consortium: Uniprot: The universal protein knowledgebase in 2023. Nucleic Acids Res 51: D523-D531, 2023.
16. Cantalapiedra CP, Hernández-Plaza A, Letunic I, Bork P and Huerta-Cepas J: eggNOG-mapper v2: Functional annotation, orthology assignments, and domain prediction at the metagenomic scale. Mol Biol Evol 38: 5825-5829, 2021.
17. Kanehisa M, Furumichi M, Tanabe M, Sato Y and Morishima K: KEGG: New perspectives on genomes, pathways, diseases and drugs. Nucleic Acids Res 45: D353-D361, 2017.
18. Oka T, Akazawa H, Naito AT and Komuro I: Angiogenesis and cardiac hypertrophy: Maintenance of cardiac function and causative roles in heart failure. Circ Res 114: 565-571, 2014.
19. Wu X, Xu M, Geng M, Chen S, Little PJ, Xu S and Weng J: Targeting protein modifications in metabolic diseases: Molecular mechanisms and targeted therapies. Signal Transduct Target Ther 8: 220, 2023.
20. Cockram PE, Kist M, Prakash S, Chen SH, Wertz IE and Vucic D: Ubiquitination in the regulation of inflammatory cell death and cancer. Cell Death Differ 28: 591-605, 2021.
21. Qiu M, Chen J, Li X and Zhuang J: Intersection of the ubiquitin-proteasome system with oxidative stress in cardiovascular disease. Int J Mol Sci 23: 12197, 2022.
22. Liu H, Zhou Z, Deng H, Tian Z, Wu Z, Liu X, Ren Z and Jiang Z: Trim65 attenuates isoproterenol-induced cardiac hypertrophy by promoting autophagy and ameliorating mitochondrial dysfunction via the Jak1/Stat1 signaling pathway. Eur J Pharmacol 949: 175735, 2023.
23. Wu L, Jia M, Xiao L, Wang Z, Yao R, Zhang Y and Gao L: TRIM-containing 44 aggravates cardiac hypertrophy via TLR4/NOX4-induced ferroptosis. J Mol Med (Berl) 101: 685-697, 2023.
24. Lee JM, Hammarén HM, Savitski MM and Baek SH: Control of protein stability by post-translational modifications. Nat Commun 14: 201, 2023.
25. Song L and Luo ZQ: Post-translational regulation of ubiquitin signaling. J Cell Biol 218: 1776-1786, 2019.
26. Liu P, Cong X, Liao S, Jia X, Wang X, Dai W, Zhai L, Zhao L, Ji J, Ni D, *et al*: Global identification of phospho-dependent SCF substrates reveals a FBXO22 phosphodegron and an ERK-FBXO22-BAG3 axis in tumorigenesis. Cell Death Differ 29: 1-13, 2022.
27. Zhu GW, Chen H, Liu SY, Lin PH, Lin CL and Ye JX: PPM1B degradation mediated by TRIM25 ubiquitination modulates cell cycle and promotes gastric cancer growth. Sci Rep 15: 6160, 2025.
28. Barbour H, Nkwe NS, Estavoyer B, Messmer C, Gushul-Leclaire M, Villot R, Uriarte M, Boulay K, Hlayhel S, Farhat B, *et al*: An inventory of crosstalk between ubiquitination and other post-translational modifications in orchestrating cellular processes. iScience 26: 106276, 2023.
29. Wang L, Zhang X, Lin ZB, Yang PJ, Xu H, Duan JL, Ruan B, Song P, Liu JJ, Yue ZS, *et al*: Tripartite motif 16 ameliorates nonalcoholic steatohepatitis by promoting the degradation of phospho-TAK1. Cell Metab 33: 1372-1388.e7, 2021.
30. Dorn GN II and Force T: Protein kinase cascades in the regulation of cardiac hypertrophy. J Clin Invest 115: 527-537, 2005.
31. Li L, Chen Y, Doan J, Murray J, Molkentin JD and Liu Q: Transforming growth factor β-activated kinase 1 signaling pathway critically regulates myocardial survival and remodeling. Circulation 130: 2162-2172, 2024.
32. Xie M, Zhang D, Dyck JR, Li Y, Zhang H, Morishima M, Mann DL, Taffet GE, Baldini A, Khoury DS and Schneider MD: A pivotal role for endogenous TGF-beta-activated kinase-1 in the LKB1/AMP-activated protein kinase energy-sensor pathway. Proc Natl Acad Sci USA 103: 17378-17383, 2006.
33. Hirata Y, Takahashi M, Morishita T, Noguchi T and Matsuzawa A: Post-translational modifications of the TAK1-TAB complex. Int J Mol Sci 18: 205, 2017.
34. Xu YR and Lei CQ: TAK1-TABs complex: A central signalosome in inflammatory responses. Front Immunol 11: 608976, 2021.
35. Hu MM, Yang Q, Zhang J, Liu SM, Zhang Y, Lin H, Huang ZF, Wang YY, Zhang XD, Zhong B and Shu HB: TRIM38 inhibits TNFα- and IL-1β-triggered NF-κB activation by mediating lysosome-dependent degradation of TAB2/3. Proc Natl Acad Sci USA 111: 1509-1514, 2014.
36. Kim K, Kim JH, Kim I, Seong S and Kim N: TRIM38 regulates NF-κB activation through TAB2 degradation in osteoclast and osteoblast differentiation. Bone 113: 17-28, 2018.
37. Uhlén M, Fagerberg L, Hallström BM, Lindskog C, Oksvold P, Mardinoglu A, Sivertsson Å, Kampf C, Sjöstedt E, Asplund A, *et al*: Proteomics. Tissue-based map of the human proteome. Science 347: 1260419, 2015.
38. Stelzer G, Rosen N, Plaschkes I, Zimmerman S, Twik M, Fishilevich S, Stein TI, Nudel R, Lieder I, Mazor Y, *et al*: The genecards suite: From gene data mining to disease genome sequence analyses. Curr Protoc Bioinformatics 54: 1-30, 2016.